Published in Fresenius' Journal of Analytical Chemistry 371, issue 2, 261-269, 2001
which should be used for any reference to this work

Multi-layer microfluidic glass chips for microanalytical applications

Antoine Daridon · Valia Fascio · Jan Lichtenberg · Rolf Wütrich · Hans Langen · Elisabeth Verpoorte Nico F. de Rooij

Abstract A new, versatile architecture is presented for microfluidic devices made entirely from glass, for use with reagents which would prove highly corrosive for silicon. Chips consist of three layers of glass wafers bonded together by fusion bonding. On the inside wafer faces a network of microfluidic channels is created by photolithography and wet chemical etching. Low dead-volume fluidic connections between the layers are fabricated by spark-assisted etching (SAE), a computer numerical controlled (CNC)-like machining technique new to microfluidic system fabrication. This method is also used to form a vertical, long path-length, optical cuvette through the middle wafer for optical absorbance detection of low-concentration compounds. Advantages of this technique compared with other, more standard, methods are discussed.

When the new glass-based device for flow-injection analysis of ammonia was compared with our first-generation chips based on silicon micromachining, concentration sensitivity was higher, because of the longer path-length of the optical cuvette. The dependence of dispersion on velocity profile and on channel cross-sectional geometry is discussed. The rapid implementation of the devices for an organic synthesis reaction, the Wittig reaction, is also briefly described.

Introduction

The original impetus for the work presented here was the development of a new, miniaturized, chemical sensing system for monitoring and process control of wastewater and drinking water. The ions of interest are primarily nitrate, orthophosphate, and ammonium, but potentially also other pollutants such as heavy metals. Analysis of these species is based on the integration of well-established wet chemical methods into automated flow systems, with absorbance detection of the resulting complexes. Chief among the challenges that needed to be met in this project were reduced reagent consumption (<1 L $year^{-1}$, or <2 μL min^{-1} for a continuously flowing system and analysis every few minutes), low detection limits (<0.5 ppm), and construction of a system sufficiently robust to operate autonomously for long periods of time without servicing. The choice of a microfluidic-based system was motivated primarily by the need to reduce reagent consumption. The microfluidic manifold was first optimized for the colorimetric detection of ammonium by the Berthelot reaction [1]. This reaction consists of three consecutive steps. The first is the chlorination of ammonia with hypochlorite (OCl^-) at high pH to form monochloramine (NH_2Cl). NH_2Cl then reacts with phenol to yield the intermediate, benzoquinonechlorimine (C_6H_4ONCl). Further reaction with phenol results in the blue-colored compound, indophenol ($C_{12}H_8O_2N$). The reaction is the basis of many sensitive and selective methods for determination of ammonium [2, 3, 4, 5].

The integration of the Berthelot reaction for determination of ammonium into a microfluidic system for use in a water-monitoring application has already been described [6, 7]. The first generation of devices, consisting of a silicon chip with dry-etched channels sandwiched between two Pyrex chips, proved the feasibility of the microfluidic approach [8]. At the flow rates used in these devices (μL min^{-1}), flow velocity profiles have the parabolic shape typical of pressure-driven laminar flow. Streamlines are straight and well defined, so mixing of adjacent sample and reagent streams depends exclusively on radial diffusion perpendicular to the direction of flow. Despite the relative slowness of this molecular transport process, it was found that the use of narrow, deep channels (30 μm wide and 200 μm deep) to minimize the distances species needed to travel enabled efficient mixing by diffusion [6]. Complete mixing of two reagent streams flowing side by

A. Daridon · J. Lichtenberg · E. Verpoorte (✉) · N.F. de Rooij
Samlab, Institute of Microtechnology, University of Neuchâtel,
2007 Neuchâtel, Switzerland
e-mail: sabeth.verpoorte@unine.ch

V. Fascio · R. Wütrich · H. Langen
DMT-ISR, Swiss Federal Institute of Technology Lausanne,
1015 Lausanne EPFL, Switzerland

side could be accomplished in less than 0.5 s. The issue of sample-zone dispersion was also considered in these first devices, because more peaks can be distinguished per unit time (or more samples analyzed) if sample zone dispersion can be minimized. As expected, peak broadening was found to increase at higher flow rates, as the parabolic profile became more pronounced and the difference between maximum and minimum flow rates across the channel became larger. Dispersion of the sample zone arising from the parabolic profile could, however, also be reduced compared with conventional systems, because radial diffusion becomes more significant in microchannels and can counteract dispersion in the direction of flow. Despite the successful integration of ammonium analysis into a microfluidic device, the use of silicon as a substrate material was not compatible with the highly alkaline reagents (pH>12.5). This is because silicon is rapidly etched at high pH [9]. Deposition of pinhole-free protective layers of silicon nitride or oxide to prevent attack proved difficult, particularly in the narrow and deep channels comprising the microfluidic network. Apart from the fact that this corrosion ultimately destroys the microfluidic structure, it induces several additional problems, e.g. the formation of gas bubbles in the channels and increased volume of the reaction coil. Increased surface roughness can also result, leading to perturbation of the parabolic flow profile, and hence greater dispersion of the sample zone in the flowing buffer stream. Prevention of these effects would improve the lifetime of microfluidic systems in corrosive environments.

In this paper, we report the design and fabrication of new, three-dimensional microfluidic structures consisting of three stacked and bonded glass chips. Several advantages are associated with this type of device. Firstly, the chemical stability of the chip is drastically improved by using glass as substrate material. Secondly, additional freedom in the lay-out of the channel network over different levels enables integration of complex fluidic manifolds into a small area. Thirdly, the middle wafer can be used to incorporate a vertical optical cell for absorbance measurements at long optical path-lengths with simple interfacing to optical fibers. For the current application, there is a need for a small-volume chip (2 μL) and long reaction times (2 min) to allow for development of the colored species. This requires long, narrow channels with a correspondingly reduced detector volume, as pointed out by van der Linden [10]. The fabrication of a low-volume detector with a long path-length is, therefore, one of the challenges to be met in the successful fabrication of the microfluidic device. Deep reactive-ion-etching (DRIE) can be used to fabricate narrow holes through silicon chips [11], but DRIE is not yet sufficiently developed for producing similar structures in quartz or glass. Use of wet-etching to produce holes through glass is also not applicable, because this is an isotropic process, producing structures which are twice as wide as they are deep. An alternative technique for drilling small holes (<200 μm diameter, volume below 0.02 μL), with a high aspect ratio through a 525 μm-thick glass wafer had to be found. This report will focus on these fabrication issues, especially the use of the spark-assisted etching (SAE) technique used for drilling [12], and on techniques for reliably interfacing microfluidic systems to the macroscopic world. It was possible to set up the resulting system as a continuous flow system for a chemical synthesis application over the course of a day, demonstrating its flexibility of use. The synthesis chosen as an example is the Wittig reaction for preparation of nitrostilbene ester compounds [13] by reaction of phosphonium salts with aldehydes.

Experimental

Reagents

Berthelot reaction

Reagents and standards for the determination of ammonium using the indophenol blue method were of analytical reagent grade and used without further purification.

Before the ammonium stock solution (100 ppm) was prepared, ammonium chloride was dried for 24 h in a desiccator. Dry NH_4Cl (Merck 1.01145, 0.382 g) was weighed and diluted to 1 L with Milli-Q water to produce a stock solution with an ammonium concentration of 7.14 mmol L^{-1}. Ammonium working standards were prepared from this stock solution by serial dilution.

Reagent 1: Potassium sodium tartrate ($KNaC_4H_4O_6$, Merck 1.08087, 30 g L^{-1}); sodium hydroxide (Merck 1.06498, 12 g L^{-1}); EDTA (Merck 1.08418, 4 g L^{-1}). EDTA and tartrate ($CO_2CH(OH)CH(OH)CO_2^{2-}$) are used to complex metal ions (i.e. Mg^{2+}, Ca^{2+}), thereby preventing formation of precipitates; pH 12.5.

Reagent 2: Phenol (Merck 1.00206, 40 g L^{-1}); sodium nitroprusside ($Na_4Fe(CN)_5ONO$, a nitropentacyanoferrate compound; catalyst, Merck 1.06541, 0.6 g L^{-1}); pH 4.9.

Reagent 3: Sodium hypochlorite (Fluka 42,504-4, 66.7 g L^{-1}, 13% active chlorine); sodium hydroxide (2 g L^{-1}), oxidizing agent; pH 12.3.

N.B. Reagents 2 and 3 are light sensitive and were stored in the dark.

Wittig reaction reagents

Solution 1: (2-Nitrobenzyl)triphenylphosphonium bromide monohydrate (Clariant 5650), 0.01 mol L^{-1} in dry degassed methanol.

Solution 2: Premixed solution of methyl 4-formyl benzoate (Clariant 10675, 0.01 mol L^{-1}) and sodium methoxide (Aldrich 40,306-7, 0.015 mol L^{-1}) in dry degassed methanol.

Microsystem test set-up

The test bench for the microfluidic FIA device included high-precision syringe pumps to drive the reagents through the chip, a fiber-optic-based spectrophotometer, a chip holder with fluidic and optical connections, and a computer for data acquisition and process control.

Two computer-controlled precision syringe pumps (Harvard Apparatus, Holliston, MA, USA; model PHD 2000) and glass syringes with connectors for standard fittings (ILS, Stützerbach, Germany) were chosen for supplying reagents and samples to the chip. For measurement of the absorption of the solution passing through the on-chip optical cell, a portable CCD spectrophotometer (Ocean Optics, Dunedin, FL, USA; model S2000) and a tungsten halogen light source were connected via optical fibers (100 μm core) to the chip holder.

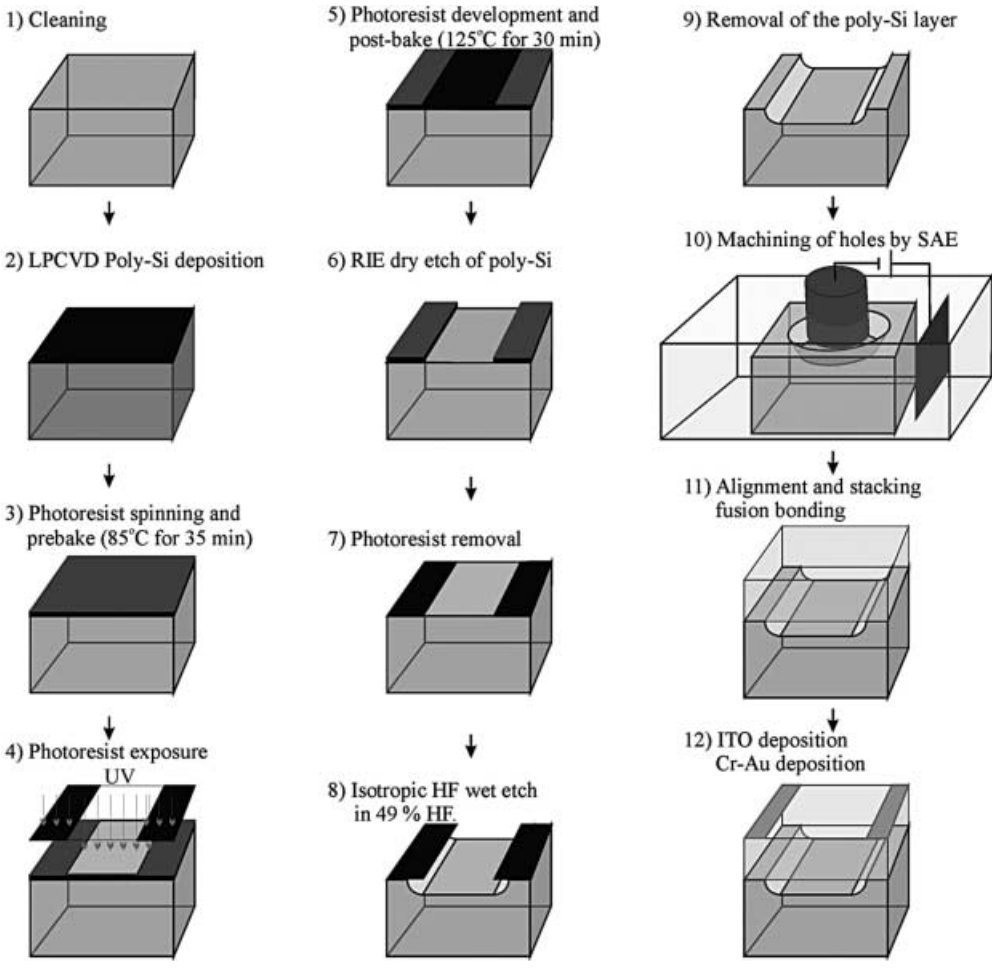

Fig. 1 Step-by-step schematic diagram of glass chip fabrication

Microfluidic chip fabrication

The assembly of a stack of glass wafers containing etched channels and drilled holes forms the microfluidic devices. Each layer is made of a double-sided-polished, 100-mm-diameter, 525-μm-thick, Pyrex 7740 wafer (Corning, NY, USA). A schematic diagram of step-by-step fabrication of the microfluidic chip is presented in Fig. 1.

Step 1: The wafers used to fabricate the channel network are thoroughly cleaned. They are first rinsed with organic solvents (acetone and isopropanol) to remove traces of organic residue from the fabrication process, rinsed with doubly distilled de-ionized water (DI water), dried in a spin washer, dipped in 100% HNO_3 for 10 min to remove any remaining organic residues left on their surface, rinsed with DI water again, and dried.

Step 2: A 200-nm-thick layer of poly-silicon is deposited on the wafer by low-temperature, low-pressure chemical vapor deposition (LPCVD). This process is conducted at 570 °C to prevent deformation and loss of planarity of the wafers. This layer protects the Pyrex surface during subsequent wet etching of glass with 49% hydrofluoric acid (HF).

Step 3: The wafer surface is then dehydrated at 200 °C for 30 min and treated for 10 min with hexamethyldisilazane (HMDS) in the gas phase. HMDS passivates the surface silanol groups (SiOH) and improves adhesion of the photoresist, a 1.8-μm thick layer of AZ-1518 positive photoresist (Clariant, Muttenz, Switzerland) which is spun on the wafer. The photoresist thickness depends on the rotation speed of the wafer, in this work 4000 rpm for 40 s. After a 30 min pre-bake at 85 °C, most of the solvents present in the photoresist have evaporated and the polymer layer becomes harder.

Step 4: The resist is exposed to near-UV radiation (365 nm) through an optical chromium mask to transfer the channel network onto the wafer.

Step 5: The photoresist is developed in an alkaline solution of 3:1 water–developer (AZ 351 B; Clariant, Muttenz, Switzerland). Only the photoresist exposed to the UV light dissolves in the solution; the rest remains on the surface (this would be the inverse for a negative photoresist). The patterned photoresist layer is then post-baked at 125 °C for 30 min to harden it.

Step 6: Reactive-ion-etching (RIE) is used to open the unprotected areas of the poly-silicon layer, thus exposing the bare glass surface where channels should be formed.

Step 7: The remainder of the photoresist is subsequently removed using acetone. The wafer is then rinsed in acetone, isopropanol, and DI water.

Step 8: The dried wafer is then carefully immersed in 49% HF solution to etch the glass surface where the poly-silicon mask was opened. The etching time depends on the rate of etching of the HF bath, which is approximately 10 μm min^{-1} at room temperature for Pyrex 7740. This wet etching is isotropic, meaning that the etch rate does not depend on the direction, and lateral and vertical etching rates are therefore the same. This is why the cross-section of the channels has this particular D-shaped profile. Final channel widths measured at the substrate surface are approximately twice the depth, plus the width of the original opening in the poly-silicon layer.

Step 9: The poly-silicon is dissolved in 40% KOH solution at 60 °C. This process is very fast, taking only approximately 1 min to remove the poly-silicon layer.

Up to this step, this process is a standard process in our laboratory for fabrication of microfluidic devices [14, 15].

Step 10: The low-volume, long-path-length optical cuvette is fabricated by localized etching of the glass by SAE through the entire wafer thickness. More details on this technique are given below.

Step 11: To interconnect the various fluidic elements (inlets, outlet, optical cuvette, and microfluidic manifold), the three wafers are aligned by use of micropositioners and a microscope, and stacked. The intermediate wafer and the bottom wafer (where the channels are etched) are aligned first and kept aligned by means of the capillary forces induced by a thin layer of water drawn between the wafers, by capillary action. The third wafer is then aligned with the other two and also fixed by introduction of a drop of doubly distilled, dust-free water. The system consists of three wafers in which the optical cuvette is a through-hole located in the intermediate layer and the upper and lower wafers are used to close the cuvette. The bottom layer includes the microfluidic manifold and the inlet holes connected to the pumps and the outlet hole. The top wafer is used to close the optical cuvette and to guide the liquids to the outlet. Once aligned, the three wafers are hermetically sealed using a thermal fusion bonding procedure at 650 °C [14].

Step 12: Because the chemical reaction used in these microfluidic chips is slow [5], an indium tin oxide layer is sputtered on top of the chip and used as a resistive heater to increase the reaction rate [6, 7]. A stable electrical contact is ensured by evaporation of 200-nm-thick gold strip electrodes over a 10- to 20-nm-thick chromium adhesion layer. Areas of the surface that do not need to be coated are masked with Scotch removable Magic tape. Once processed, the bonded wafers are diced into 2.3 cm×2.3 cm× 0.15 cm large chips. These microfluidic devices are mounted in a special chip holder made of poly(methyl methacrylate) (PMMA) containing a number of fluidic ports, two SMA-compatible mounts for optical fibers, two electrical contacts, and a Pt-100 element for temperature monitoring. Reliable fluidic interconnections between the syringes and the chip holder are ensured by use of PEEK tubing (1/8" o.d., 0.02" i.d.) and pressure-tightened, flangeless ferrules (Upchurch Scientific, Oak Harbor, WA, USA) integrated into the PMMA holder. A picture of the chip holder with a chip mounted is shown in Fig. 2. This configuration enables rapid mounting and removal of chips, with chips simply placed into a slight recess formed in the lower block of the holder before assembly of the holder. The dimensions of this recess are similar to those of the chip itself, so that it sits snugly in place. Positioning the chip in the holder in this way also enables precise alignment of the access holes in the chip with the fluidic connections. The upper and lower parts of the holder are made from 2-cm-thick PMMA. This thickness is needed to avoid bending of the holder, which could apply uneven pressure to the chip, resulting in breakage during the mounting process. A closer view of this connection is presented on the right in Fig. 2. In this figure, the vertical optical cuvette fabricated by SAE through the Pyrex chip is clearly visible. The channels into and out of the cuvette are seen at the bottom left and the top right, of the cuvette, respectively, due of the diffraction of light on their surfaces.

Results

Figure 3 depicts an optical cuvette machined by SAE. This hole has a diameter of 200 μm through a 525-μm-thick wafer. This localized etching method was chosen because it can be used to drill small holes into an amorphous material like glass, which is required for the fabrication of the low dead-volume optical cuvette. SAE does not produce particles and can be used on wafers on which the channels are already etched. Particles produced by mechanical or ultrasonic drilling are not compatible with the bonding procedure, because they are difficult to remove. Ultrasonic drilling also does not permit the fabrication of such small holes. High-pressure water-jet drilling suffers from the same limitation. The edges of the holes on the attack side are very rough, and even post-drilling chemical smoothing of the surface is not applicable [16]. Isotropic wet etching in HF (in house) was not an option, because the diameter of the through-hole would have been twice the wafer thickness (i. e. >1 mm) if etched from one side. This could be improved if holes were etched simultaneously from both sides of the wafer to meet in the middle, but through-hole diameter would still be approximately 500 μm. Another possibility that was investigated was the use of previously processed wafers in which holes had been drilled before polishing (Sensor Prep Services, Elburn, IL, USA). This approach was again not applicable, because of the large dimensions of the holes (500 μm). Patterning channels on previously drilled wafers also poses a problem – the presence of the holes prevents uniform resist distribution during spin-coating. This affects the design of the channel network in an unacceptable manner, with effects like barriers in the channels, interconnection of adjacent channels and increased channel side-wall roughness being observed. The use of a pho-

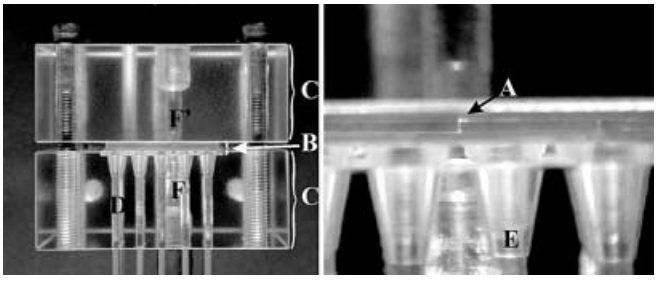

Fig. 2 (*left*) Photograph of the microfluidic chip and chip-holder. (*Right*) Close up view of the microfluidic chip, microfluidic connections, and optical connections. *A*, Optical cuvette drilled by SAE; *B*, Microfluidic chip made of three Pyrex layers; *C*, PMMA plates; *D*, PEEK tubing, 0.020" i.d.×1/16" o.d.; *E*, flangeless ferrule, 1/16"; *F*, *F'*, Collection and illumination optical fibers, respectively

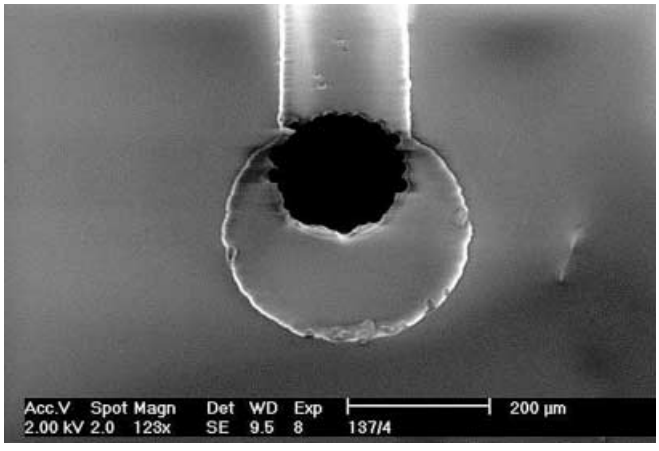

Fig. 3 SEM image of an optical cuvette etched by SAE at the end of a 200-μm-wide channel wet-etched in HF

toetchable glass, Foturan (Schott Glasswerke, Germany), was considered. After regions of a Foturan wafer are exposed to light and cured, their etch rate in HF is 20 times higher than for unexposed glass. The minimum diameter for a through-hole in a 500 μm thick wafer is approximately 75 to 100 μm [17, 18]. However, Foturan wafers undergo a change in their bulk structure during curing, and subsequent re-polishing before fusion bonding is required, which complicates the fabrication procedure considerably.

In the SAE process, the glass plate to be machined is submersed in an electrolyte solution (30% NaOH) in an electrochemical cell. The anode is a platinum wire in a ring shape around the drilling site, while the needle-like cathode acts as machining tool, as shown in Fig. 1, Step 10. By applying a constant voltage between these electrodes, sparks are generated at the surface of the cathode, which erode the glass. The high-temperature chemical reaction associated with the erosion of glass is:

$$2Na^{+}_{(aq)}+SiO_2+2OH^{-}_{(aq)} \rightleftharpoons Na_2SiO_{3(aq)}+H_2O \qquad (1)$$

There is no need to use a mask in this process, because erosion occurs only in the vicinity of the cathode in an approximately 25 μm diameter region with an applied voltage of 30 V [19]. The average vertical machining speed is approximately 30 μm s^{-1}. Erosion slows as the hole gets deeper, probably because of the slower replenishment of electrolyte at the bottom of the hole. Erosion would eventually stop if the electrolyte was not renewed by moving the tip 50 to 100 μm up and down on a regular basis, every 5 s. The hole diameter depends directly on the diameter of the tool, the cathode. It is therefore only possible to drill small holes with the use of very fine tools. In this case, 100-μm-diameter needles were fabricated by wire electro-discharge grinding (in-house prototype) [20, 21], and were used to pierce 200 μm diameter holes through a 525-μm-thick wafer, as depicted in Fig. 3. The wall aspect ratio for this hole was estimated to be 25:1, because the hole radius decreased by approximately 1 μm for every 25 μm etched into the wafer.

Each device has four inlets, one for the sample and one for each of the reagents of the Berthelot reaction, and a single outlet that leads to the waste reservoir. The syringes containing the reagents are all mounted on the same syringe pump, so that the three are always delivered at the same flow rate. The syringe containing the sample is mounted on the second pump. Figure 4 is an exploded schematic view of the microfluidic chip, with the three glass chips represented. The channels etched in the chips are wide (200 μm in the plane of the chip) and shallow (30 or 60 μm perpendicular to the plane of the chip). In the microfluidic network, the sample is mixed first with reagent 1, then with reagent 2 and finally with reagent 3. The reagents are added from under the chip, then passed through a channel etched in the bottom of the middle chip and back down to the microfluidic network. Mixing is based on diffusion under laminar flow conditions, which dominate in these chips. The solutions are therefore added one on top of the other in the shallow channels to minimize the distance molecules must diffuse to ensure complete mixing. If reagent addition were performed from side channels in the plane of the main channel width, the time needed for complete mixing would be much longer. Between each addition there is a mixing coil; these are short to minimize dispersion but sufficiently long to ensure full mixing. After the addition of reagent 3 there is a long reaction coil, to enable full development of the reaction product before reaching the optical cuvette. The channel meander was therefore designed as a compromise between low dispersion, low flow resistance, and short mixing times [11, 22]. For a given chip volume, the wider the channels, the shorter the reaction coil. This results in lower flow resistance, but also larger dispersion and longer mixing time. By reducing the channel width, it is possible to reduce dispersion and mixing time in the microfluidic manifold, but the pressure increases rapidly, an important issue if one wants to remain within the limits of pump performance.

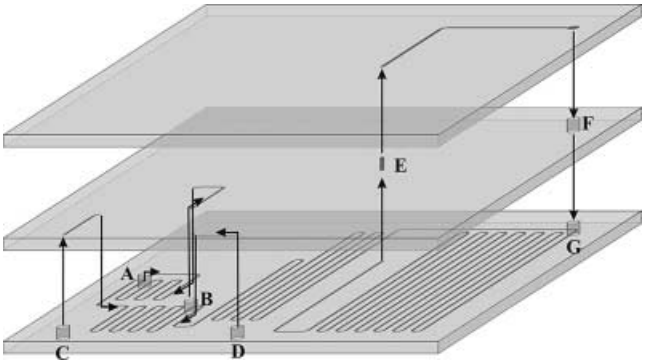

Fig. 4 Exploded view of the three layers of the microfluidic chip. The channels, inlets, and outlets are located in the bottom wafer; the optical cuvette is etched in the intermediate layer. Outlet channels for the cuvette are found in the top wafer. The etched channels are drawn in gray and the black arrows show the direction of solution flow from the inlets via the optical cell to the outlet. *A*, sample inlet; *B*, reagent 1; *C*, reagent 2; *D*, reagent 3; *E*, optical cuvette; *F*, connection, cover plate to bottom plate; *G*, outlet to waste

Calibration plots obtained for two generations of microfluidic chip are compared in Fig. 5. In one instance the microfluidic chip was composed of three stacked layers of Pyrex and the optical cuvette was etched by SAE (optical path-length 585 μm, diameter 200 μm). In the second instance, considered in a previous study [6], a silicon wafer was sandwiched between two Pyrex wafers, and the optical cuvette was etched in the silicon layer by DRIE (optical path-length 400 μm, diameter 200 μm). In these experiments, the ammonium standards and reagents were premixed off-chip and the mixture was added into the chip after completion of the reaction. Using one of the reagent inlets, DI water was added to the mixture to dilute the standard solution in the chip. The two curves of Fig. 5 show a large linear dynamic range from 0.2 to 20 ppm. The slopes lead to estimated values of the extinction coefficient of 19,170 mol^{-1} cm^{-1} L (standard deviation 900 mol^{-1} cm^{-1} L) and 20,060 mol^{-1} cm^{-1} L (standard de-

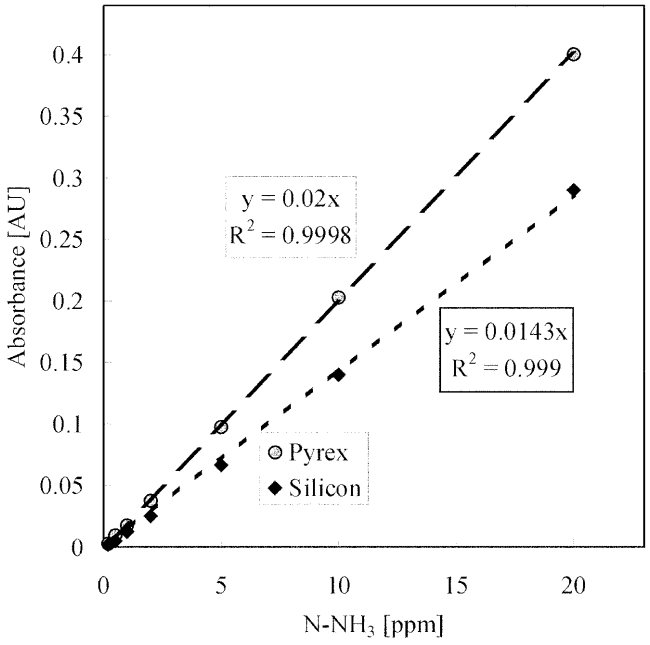

Fig. 5 Calibration curves of absorbance at 635 nm as a function of ammonium concentration for the Pyrex and the silicon optical cuvettes, using premixed solutions containing ammonium and reagents which had been allowed to go to complete reaction. Concentrations are expressed in terms of ppm N present in the form of NH_4^+. Absorbance was measured in the optical cuvette drilled in the Pyrex wafer (525 µm thick) by SAE [8, 11] (total path-length including depths of inlet and outlet channels (30 µm each): 585 µm), and compared with the absorbance measured in a silicon optical cuvette formed by deep reactive-ion-etching (optical path-length: 400 µm) [7]

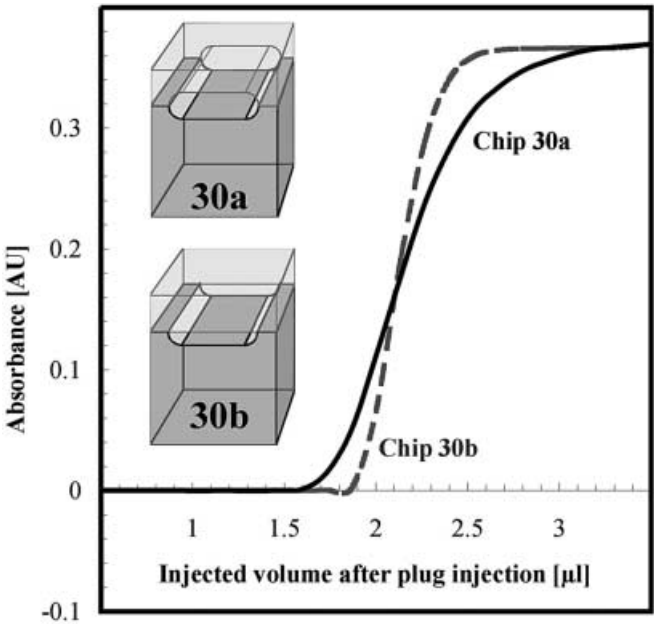

Fig. 6 Initial part of the absorbance profile of indophenol blue solution plugs for two different geometries. Large plugs were injected to obtain the maximum signal, with the result that absorbance plateaus rather than Gaussian peaks are recorded. Total flow rate: 8 µL min^{-1}. The ammonia was converted into indophenol blue off-chip and the initial concentration of the solution was 17 ppm. The dispersed volume is calculated from the area under the absorbance peak between dye–carrier mixing ratios of 3%:97% and 97%:3%

viation 1200 mol^{-1} cm^{-1} L) for the Pyrex and silicon micro-optical cuvettes, respectively. These values compare well with data acquired on a conventional spectrophotometer, in-house (20,600 mol^{-1} cm^{-1} L, standard deviation 850 mol^{-1} cm^{-1} L) and by Boletter et al. in 1961 (18,700 mol^{-1} cm^{-1} L, standard deviation 150 mol^{-1} cm^{-1} L) [4, 6].

For the Pyrex chip, no pinhole was necessary to prevent a large background signal from scattered light or stray light around the cuvette itself. The optical cables used in the set-up have an SMA connector with an opening of 100 µm, so the light-collecting fiber only receives light that has passed through the cuvette if both fibers are precisely aligned. Aligning the optical fibers with the cuvette was easy as their cores are much smaller than the cuvette diameter, leaving a margin of 50 µm around the opening.

Two channel geometries were processed in glass to study dispersion (sample zone broadening) in the microfluidic chip. For the first, the channel was formed by etching into one chip face only. After bonding to the Pyrex cover plate, the channel had a D-shaped cross-section as presented schematically in Fig. 6, drawing 30b. For the second geometry, channels were etched on opposing faces, so that after aligning and bonding, the channel had an oval cross-section as shown in drawing 30a of Fig. 6. In both instances the wafers were etched to 30 µm in depth and the width of the channels after processing was 200 µm, which, for 30a, gave channels 60 µm high and 200 µm wide. To maintain the reaction coil volume constant at 2 µL for the two designs, 30a and 30b, the length of channel 30a was one half that of channel 30b. A summary of the typical channel dimensions of chip 30a and chip 30b is given in Table 1. Following the same experimental protocol as described elsewhere [11], these two different geometries were studied with respect to the dispersion that they induce. During the experiments the total flow rate in the chip was kept constant. A dye solution (indophenol blue solution prepared off-chip) was injected during a period of time T, during which the dye and carrier pumps ran simultaneously; this period of time defines the volume of the plug in the carrier stream. After T, only the pump delivering the carrier was operated for a period of time sufficient to rinse the optical cell. The absorbance of the dye was measured when the plug formed during T passed through the optical cell. Fig. 6 shows the ab-

Table 1 Intrinsic chip and channel properties

Chip	V_{chip} (µL)	Depth, d (mm)	Width, w (mm)	L (mm)	A (mm^2)	t_{diff}[a] (s)
30a	2	0.06	0.2	178	0.0112	3.6
30b	2	0.03	0.2	356	0.0056	0.9

[a]Calculation based on a diffusion coefficient: $D=10^{-9}$ m^2 s^{-1}

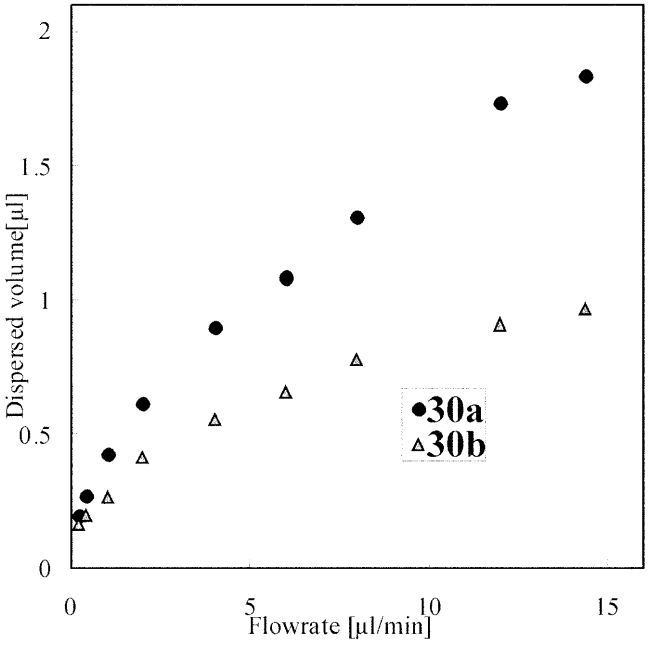

Fig. 7 Dispersed volume in the microfluidic chip measured as a function of the flow rate for two different channel geometries

sorbance curves measured for a plug of indophenol blue solution injected in chips 30a and 30b under the same conditions. The dispersed volume is calculated from the area under the absorbance signal between dye–carrier volumetric mixing ratios of 3%: 97% and 97%: 3%, as described elsewhere [23]. The curves shown in Fig. 6 were recorded at a flow rate of 8 µL min^{-1} with dispersed volumes of 1.4 µL and 0.75 µL for chips 30a and 30b, respectively. Figure 7 presents two curves showing the influence of flow rate on the dispersion induced in the microfluidic chip. As expected from theory [11, 24, 25], dispersion increases with increasing flow rates. The two types of chip have different dispersion properties, with the wider chip inducing more dispersion than the narrow one under the same flow conditions. This can be explained by considering the relative magnitudes of the time for convective flow, t_{conv}, and the time for diffusion across the channel, t_{diff}, in a pressure-driven system.

The time, t_{conv}, required for a sample plug to be carried by laminar flow down a tube or channel of length, L, during which dispersion of the sample occurs because of the parabolic flow profile, is given by:

$$t_{conv} = \frac{L}{\bar{u}} = \frac{V_{chip}}{F} \tag{2}$$

t_{diff} is defined as

$$t_{diff} = \frac{d^2}{D} \tag{3}$$

where $\bar{u}$ is the average linear flow rate, V_{chip} the volume of the channel network in the chip, F the volumetric flow rate, d the channel depth and D the diffusion coefficient.

When the ratio t_{conv}/t_{diff} is larger than 1, radial diffusion is fast enough to reduce radial variations in concentration and hence reduce dispersion of the sample zone arising from the laminar flow profile. This flow regime is known as Taylor flow, after the scientist G.I. Taylor who first described it in 1953 [24]. For a given volumetric flow rate, t_{conv} is the same for the two geometries, because the chips have the same volume. At a flow rate of 5 µL min^{-1}, assuming $D=10^{-5}$ cm^2 s^{-1}, the ratio t_{conv}/t_{diff} is 6.7 and 26.7 for chips 30a and 30b, respectively. The flow rate influences many properties of the microfluidic chip, as shown by the summary for two flow rates given in Table 2. Values for (t_{conv}/t_{diff}) show that the assumption of Taylor flow is true for both geometries and that it is more pronounced for 30b. Hence, reducing channel diameters, or depths, as the case may be, also results in radial diffusion becoming a more significant means of molecular transport. Under these conditions the laminar velocity profile disperses the solute with an effective dispersion coefficient, D_{eff}, which is inversely proportional to the molecular diffusion coefficient [24, 25]. One can define this effective dispersion coefficient for channels where the width is much larger than the depth by [25]:

$$D_{\text{eff}} = \frac{33}{560} \cdot \frac{\bar{u}^2 d^2}{D} \tag{4}$$

From Eq. (4), one sees that D_{eff} is dependent not only on linear velocity, but also on channel depth. D_{eff} is thus the same for both geometries, because d_{30a} is twice d_{30b} and $\bar{u}_{30a}$ is half $\bar{u}_{30b}$. Fig. 7 shows that there is more dispersion for 30a (oval cross-section) than for 30b (D-shaped cross-section) at any given flow rate. This different dispersion is due to reduced radial diffusion in chip 30a, because the influence of laminar flow dispersion is the same in the two chips as indicated by the equal values of D_{eff}.

The experimental arrangement, including the syringe pumps, the three-way valves, tubing, chip holder, fluidic connections, and microfluidic chip have proven to be a robust and rapidly implementable system. It was possible in 3 h to perform a chemical reaction not previously tested in the system, including the preparation of the solutions and assembly of the set-up. The test chemical reaction chosen for this experiment was the Wittig reaction, which has previously been studied in an electrokinetically pumped continuous flow microsystem [13]. The Wittig reaction is a two-step reaction in which a phosphonium salt reacts with sodium methoxide to form an ylide. As reported

Table 2 Dependence of chip properties on flow rate

Chip	F (µL min^{-1})	$\bar{u}$ (mm s^{-1})	t_{conv} (s)	t_{conv}/t_{diff}[a]	D_{eff} (m^2 s^{-1})
30a	1	1.48	120	33.3	4.7×10^{-7}
	5	7.4	24	6.7	1.2×10^{-5}
30b	1	2.96	120	133	4.7×10^{-7}
	5	14.8	24	26.7	1.2×10^{-5}

[a]Calculation based on a diffusion coefficient: $D=10^{-9}$ m^2 s^{-1}

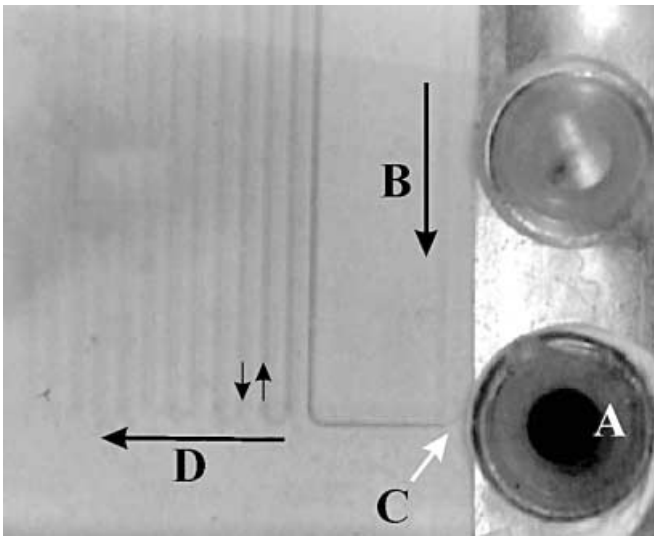

Fig. 8 Microfluidic chip used to perform the Wittig reaction. *A*, One of the two inlets used to introduce the solutions to the microfluidic chip; *B*, Channel of introduction of one reagent (second inlet outside the picture); *C*, Mixing point; *D*, The overall direction of the flow is shown by the large arrow, the small arrows show the direction of the flow in the channels. The intermediate color due to the ylide forms instantaneously, and disappears as the reaction zone progresses through the channel

elsewhere [13], if (2-nitrobenzyl)triphenylphosphonium bromide is chosen as the starting compound, the ylide is a colored compound that can be used to follow the reaction. The purple compound disappears when it has reacted with the third compound, an aldehyde, to yield a stilbene ester and a phosphine oxide. Fig. 8 shows a top view of the microfluidic chip while the Wittig reaction was running. With this particular chip, only two inlets were used. One is outside the border of the picture and the second is visible at the bottom right. Visible here is the fluidic connection, which includes the ferrule around the peek tubing, in contact with an inlet hole formed by SAE. The phosphonium salt solution and a mixed sodium methoxide–aldehyde solution are introduced from the upper and bottom inlets, respectively. The two solutions meet in a T-junction and react immediately to form an intense purple ylide intermediate. As the stilbene ester is formed, the color of the solution fades. This is visible in Fig. 8, where the color in the serpentine channel is very intense immediately after the mixing point (point C) and fades as the solution travels in the serpentine channel (towards the left). This example shows another advantage of these chips, which is the possibility of looking into the channel and having control of what is happening.

Conclusion

A new design for three-dimensional microfluidic structures consisting of three stacked, glass wafers has been presented. The use of glass substrates improves the long-term chemical stability of the device in comparison with silicon-based systems; the three-layer architecture also offers more design freedom. SAE proved to be a very useful and versatile technique for fabrication of thin, low dead-volume, liquid interconnections between layers of the chip. Furthermore, an SAE-drilled through-hole served as a long path-length optical cuvette for absorbance measurements, the length of which can, to some extent, be tailored by changing the thickness of the middle chip. The dependence of sample plug dispersion on the cross-sectional geometry of the channel could be experimentally demonstrated. Channel depth plays an especially important role when designing microfluidic FIA systems where low dispersion of the sample is needed.

Finally, a new concept for interfacing microfluidic chips with the macroscopic world, by means of a dedicated chip holder and flangeless, pressure-tight ferrules, has been presented. Chip holders based on this concept could prove to be a good choice for easily replaceable microfluidic chip modules in commercial applications, in both chemical analysis and synthesis.

Acknowledgements This work was carried out in the framework of the Brite-Euram project "MicroChem"(BE97–5134), and was financially supported by the "Office fédéral de l'éducation et de la science" in Bern, Switzerland. J. Vuille (Professor A. Shah, IMT Neuchâtel) performed ITO layer deposition. The PMMA chip holder was manufactured by Mr Balmer (mechanical workshop, Centre Suisse d'Electronique et Microtechnique S.A., Neuchâtel). AD personally acknowledges the MicroTAS team for helpful discussions and the technical staff at IMT for performing certain process steps. Dr Victoria Skelton (Microreactor Group (Professor Steven Haswell), School of Chemistry, University of Hull, UK) is gratefully acknowledged for providing her know-how in the implementation of the Wittig reaction.

References

1. Berthelot M (1859) Répert Chim Pure Appl 1:284
2. Weatherburn MW (1967) Anal Chem 39:971–975
3. Lubochinsky B, Zalta P (1954) Bull Sté Chim Biol 36:1363
4. Bolleter WT, Bushman CJ, Tidwell PW (1961) Anal Chem 33(4):392–394
5. Harfmann RG, Crouch SR (1989) Talanta 36(1/2):261–269
6. Daridon A, Sequeira M, Pennarun-Thomas G, Dirac H, Krog JP, Gravesen P, Lichtenberg J, Verpoorte EMJ, Diamond D, de Rooij NF, (2001) Sensors Actuators B 76(1–3):235–243
7. Daridon A, Sequeira M, Pennarun-Thomas G, Lichtenberg J, Verpoorte E, Diamond D, de Rooij NF (2000) Proc Eurosensors XIV, August 27–30, Copenhagen, Denmark. pp 815–818
8. Krog JP, Dirac H, Fabius B, Gravesen P, Daridon A, Lichtenberg J, Verpoorte E, de Rooij NF, Pennarun-Thomas G, Sequeira M, Diamond D, Denninger M, Geschke O, Kutter JP, Howitz S, Strec C, Charles P, Cognet L (2000) Proc μTAS 2000 Symp (Kluwer Academic), May 14–18, Enschede, The Netherlands, pp 419–422
9. Petersen KE (1982) Proc IEEE 70:420–457
10. van der Linden WE (1987) Trends Anal Chem 6(2):37–40
11. Daridon A, Gravesen P, Dirac H, Krog JP, Verpoorte E, de Rooij NF (2000) Proc μTAS 2000 Symp (Kluwer Academic), May 14–18, Enschede, The Netherlands, pp 303–306
12. Basak I, Ghosh A (1996) J. Mater Proc Technol 62:46–53
13. Skelton V, Greenway GM, Haswell SJ, Styring P, Morgan DO, Warrington B, Wong SYF (2001) Analyst 126:7–10
14. Lichtenberg J, Verpoorte E, de Rooij NF (2001) Electrophoresis 22:258–271

15. Dodge A, Fluri K, Verpoorte E, de Rooij NF (2001) Anal Chem 73(15):3400–3409
16. Diepold T, Obermeier E (1996) J Micromech Microeng 6(1):29–32
17. Dietrich TR, Abraham M, Diebel J, Lacher M, Ruf A (1993) J Micromech Microeng 2:187–189
18. Indermühle PF, Ammann E, Häring P, Kötz R, Siegenthaler H, de Rooij NF (1998) Microelectr Eng 41/42:547–550
19. Fascio V, Wüthrich R, Viquerat D, Langen H (1999) Proc Int Symp Micromechatronics and Human Science '99
20. Masuzawa T, Fujino M, Kobayashi K, Suzuki T (1985) Ann CIRP 34(1):431
21. Langen H, Breguet JM, Bleuler H, Renaud P, Masuzawa T (1998) Int J Elec Machining 3:65–69
22. Veenstra TT, Lammerink TSJ, van den Berg A, Elwenspoek MC (1998) Proc Dutch Sensor Conf (Kluwer Academic), The Netherlands, pp 263–267
23. Griffiths SK, Nilson RH (1999) Anal Chem 71(24):5522–5529
24. Taylor GI (1953) Proc R Soc Lond A (219):186
25. Beard DA (2001) J Appl Phys 89(9):4667–4669